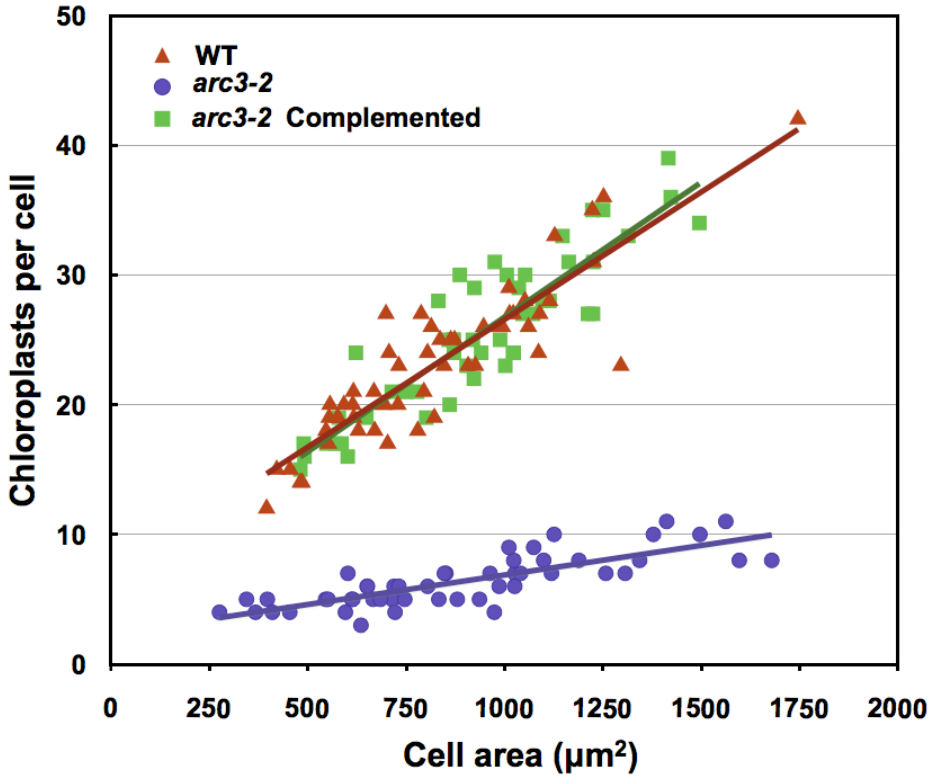

Supplemental Figure 1. Quantitative Analysis of Chloroplast Number vs. Mesophyll Cell Size in Young Expanding Leaves.

Cells from 2.5-week old seedlings of WT (Col-0), *arc3-2* and T_1 *arc3-2* transgenics complemented with *PARC3-ARC3-Myc* were quantified (n ≥ 50 cells). R^2 values for best-fit lines are 0.80, 0.64 and 0.81 for plants of WT, *arc3-2* and *arc3-2* complemented with *PARC3-ARC3-Myc*, respectively.

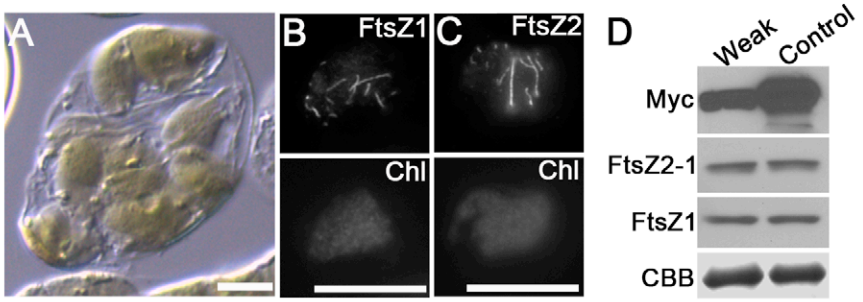

Supplemental Figure 2. Chloroplast Phenotype and FtsZ Morphology in WT Plants with Lower Accumulation of ARC3-Myc.

(A) to **(C)** Brightfield **(A)** and epifluorescence (**[B]** and **[C]**) micrographs showing the mild chloroplast division defect **(A)** and FtsZ1 and FtsZ2 filaments within chloroplasts (**[B]** and **[C]**) in a mesophyll cell of a WT plant transformed with *P35S-ARC3-Myc* and expressing the fusion protein at lower levels than in Figure 1D. Anti-FtsZ1- and anti-FtsZ2-1-specific antibodies were used for immunolabeling FtsZ1 and FtsZ2, respectively. Chl, chlorophyll autofluorescence. Scale bars, 10 μm.

(D) Immunoblot showing ARC3-Myc levels in the transgenic plant shown in (**[A]** to **[C]**). Total protein from 2 mg of fresh leaf tissue was loaded in each lane. ARC3-Myc, FtsZ1 and FtsZ2 were detected with anti-Myc, anti-FtsZ1, and anti-FtsZ2-1, respectively. Control shows the signal from the same extract as shown in Figure 1E, lane 6. CBB, Coomassie staining of Rubisco in the gel as a loading control.

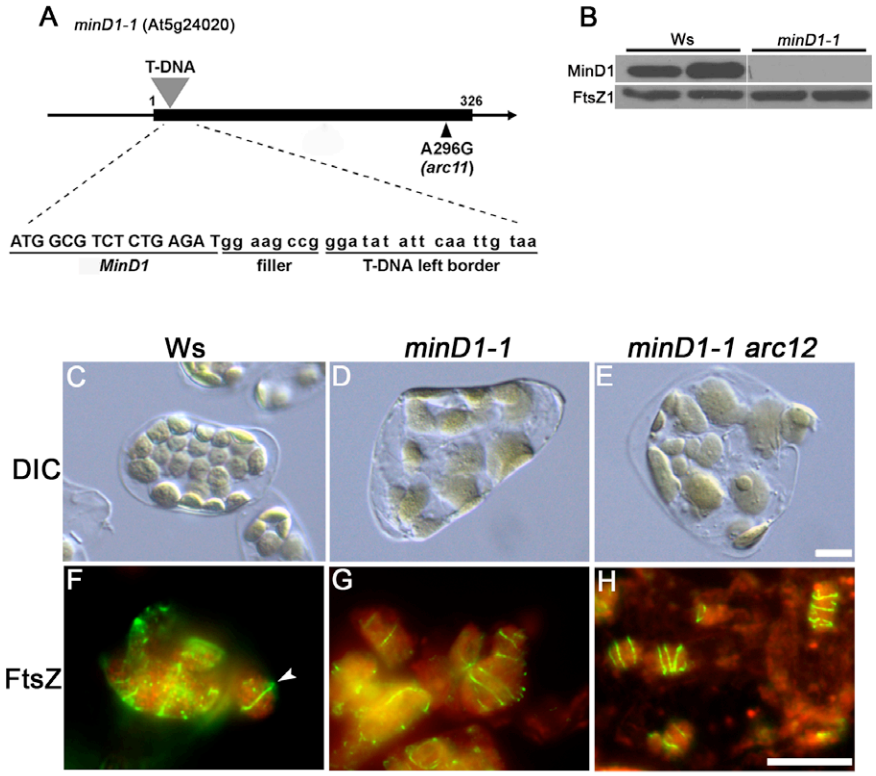

Supplemental Figure 3. Chloroplast Phenotypes and FtsZ Morphology in the *minD1-1* Single Mutant *and* the *minD1-1 arc12* Double Mutant.

(A) Structure of the *minD1-1* allele (Ws background). The T-DNA insertion (gray triangle) interrupts the *Arabidopsis MinD1* open reading frame, which encodes a 326-amino acid protein, 16-bp downstream of the translational initiation site, within the region encoding the predicted transit peptide. The sequence at the junction with nucleotides from *MinD1* (capital letters), an 8-bp linker of unknown origin (filler), and the T-DNA left border are shown. The structure of the allele indicates it is null for *MinD1*. Black triangle shows the positions of the point mutation in the *arc11* allele (Fujiwara et al., 2004).

(B) Immunoblot analysis showing *minD1-1* is a knockout mutant of *Arabidopsis MinD1.* FtsZ1 is shown as a loading control.

(C) to **(H)** Chloroplast phenotype (DIC) and FtsZ morphology in single mesophyll cells of *minD1-1* and *minD1-1 arc12*. **(F)** to **(H)** shows merged images of fluorescence signals from immunolabeling of FtsZ (green) and chlorophyll autofluorescene (red). White arrowhead indicates FtsZ ring in WT plants in **(F)**. Scale bars, 10 μm.

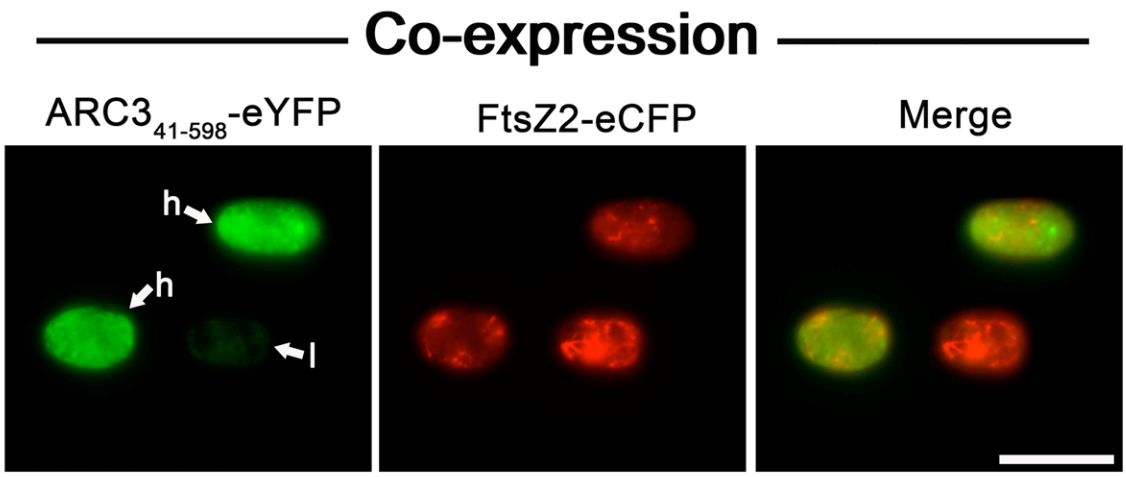

Supplemental Figure 4. FtsZ2-eCFP Morphology in Additional *S. pombe* Cells with Higher Accumulation of ARC3$_{41-598}$-eYFP.
Images were processed and labeled as described in Figure 7. Scale bar, 10 μm.

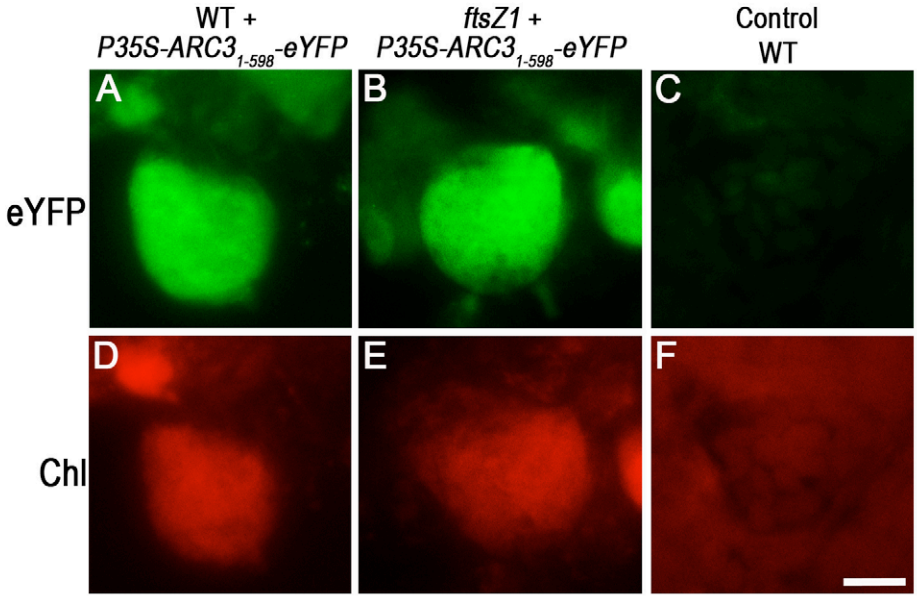

Supplemental Figure 5. Localization of ARC3$_{1-598}$-eYFP in WT and *ftsZ1* Plants.
(A) to **(B)** Localization of ARC3$_{1-598}$-eYFP in chloroplasts of mesophyll cells of WT (Col-0) plants **(A)** and *ftsZ1* plants expressing *P35S-ARC3$_{1-598}$-eYFP* **(B)**. The ARC3$_{1-598}$-eYFP signal was predominantly detected in the stroma. **(C)** Control showing lack of eYFP signal in chloroplasts of WT. Images were obtained using a 0.1 s exposure.
(D) to **(F)** Autofluorescence of chlorophyll showing chloroplast morphologies in mesophyll cells of the indicated plants. Images were obtained using a 0.01 s exposure.
Chl, chlorophyll autofluorescence. Scale bars, 10 μm.

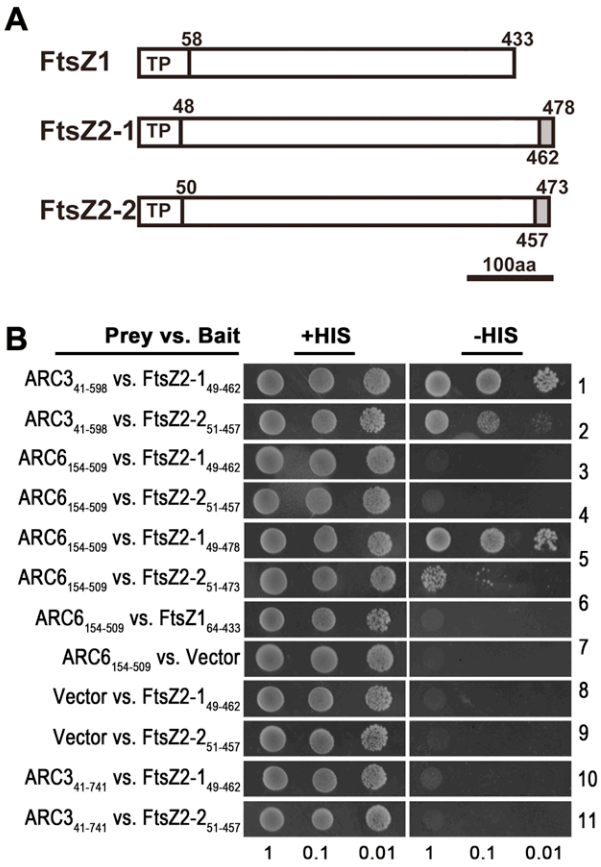

Supplemental Figure 6. Yeast Two-hybrid Assays between ARC3 and Truncated Variants of FtsZ2-1 and FtsZ2-2.

(A) Schematic diagram emphasizing the absence in FtsZ1 and presence in FtsZ2-1 and FtsZ2-2 of the conserved C-terminal peptide (gray).

(B) Yeast two-hybrid assays showing that $ARC3_{41-598}$ interacts with both FtsZ2-1 and FtsZ2-2 lacking their C-terminal peptides. Interactions between the stromal region of ARC6 (residues 154-590) and FtsZ2-1 and FtsZ2-2 with and without their C-terminal peptides, served as controls. All ARC6 and FtsZ2 vectors and interactions were reported previously (Schmitz et al., 2009).

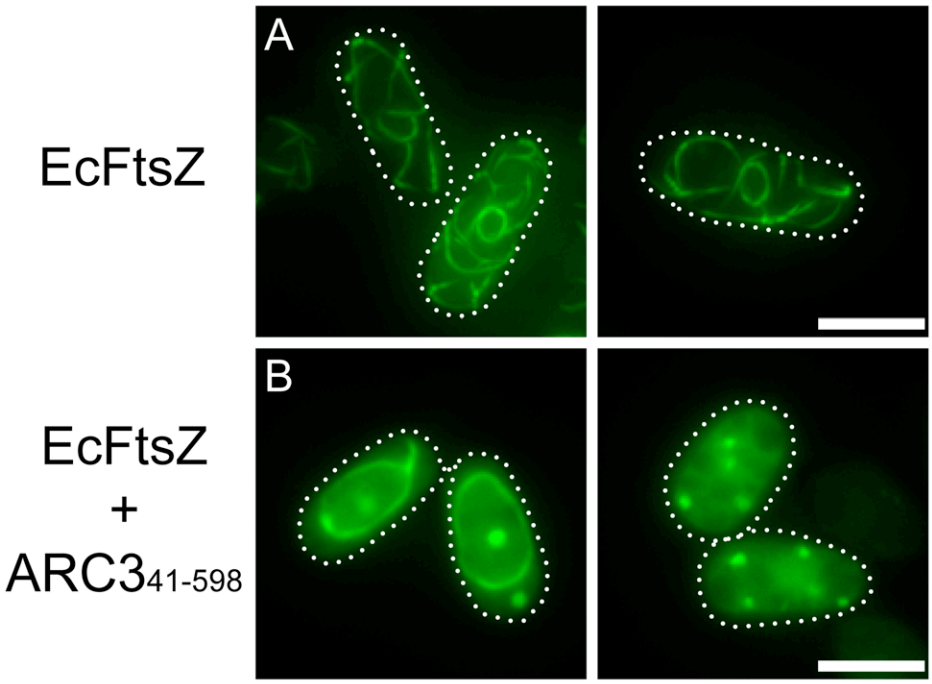

Supplemental Figure 7. Effect of ARC3$_{41-598}$ on *E. coli* FtsZ Assembly in *S. pombe*.
(A) Epifluorescence micrographs showing the morphology of *E. coli* FtsZ tagged with GFP (EcFtsZ) in *S. pombe* cells. *pREP42-FtsZ-GFP* (Srinivasan et al., 2007) was transformed into *S. pombe* strain MBY192.
(B) Morphology of EcFtsZ coexpressed with *Arabidopsis* ARC3$_{41-598}$ in *S. pombe.* Cells were transformed with both *pREP42-FtsZ-GFP* and *pREP41X-ARC3$_{41-598}$-eYFP*; the promoters in the two vectors are the same.
Images show the GFP signal from EcFtsZ-GFP falsely colored green. Scale bars, 5µm. Samples were imaged by differential interference contrast (not shown) and epifluorescence microscopy using a microscope (model DMRA2; Leica) with an HCX PL Apochromat 63x (1.32 NA) oil-immersion objective (Leica) and a camera (Retiga Exi; QImaging) at room temperature. Z stacks were taken using 0.5-µm increments, and the images were de-blurred by performing nearest neighbor deconvolution with 70% haze removal using Image-Pro 7.0 software (Media Cybernetics). White dots show cell outlines.

Supplemental Table 1. Primers Used in This Paper Shown 5' to 3'.

Name	Sequence	Enzymes
LBb1.3	ATTTTGCCGATTTCGGAAC	N/A
*ARC3*LP	AAGAAATCTATCCGCTCGAGC	N/A
*ARC3*RP	TGACCTTGTTCCATCCAAATC	N/A
*Z1*LP	CAGAGCTTGCGAATCCGTGTT	N/A
*Z1*RP	AAGCATGCGCAAAGTCAGTCG	N/A
Z2-2LP	ACCTACAAATCGTTTCCCGAG	N/A
Z2-2RP	TGGTGCTCCTATAATTGCAGG	N/A
Z2-*1*LP	TTTTCATGTAATGCTGCAAACTTC	N/A
Z2-*1*RP	ACCCCTAGTCAACTCCTTACCAAT	N/A
G-DNA	ATATTGACCATCATACTCATTGC	N/A
KOY07	CATTTTATSSTSSCGCTGCGGACATC	N/A
KOY10	ATAAACCGTAAACCCTGTGAAGCC	N/A
KOY11	CACGTTTCTTAGGTTCTTCCA	N/A
A12F	CAACATGGGTTTCTTTGACAGGTTAAACTTA	N/A
A12R	TGTTGTTGACGATTTTCCTTTTAGCTT	N/A
MZ3	GCTCTAGAATGCCGATTTCTATGGAACTTC	XbaI
MZ4	GGACTAGTCGCTTTCGGCCTTCAAAG	SpeI
MZ5	CGTCTAGAAGAGGTAGTTTTTTGTTGCT	XbaI
MZ6	GGACTAGTATCTGTACATAAGAGAGTTGAAGGATT	SpeI
MZ7	ACAGATTCTAGAAAGTTACAAAGAGGCA	XbaI
MZ19	CGAGCTCTCACAGATCCTCTTCTGAGATGAGTTTTTGTTCATC TCCGGCGTCCACTTGTT	SacI
MZ1	CCAAGCTTTCAGTGGAAGATTCAACAAGCG	HindIII
MZ2	GCTCTAGACGGCATTGCTCCGCTTC	XbaI
MZ9	CATCTTCTTACTAGTGGGCTGCTTTTTC	SpeI
MZ22	CGGTCGACAAGAATAGGACTCCATCTTTTTGAT	SalI
MZ109	GCTCTAGAATGGCGTCTCTGAGATTGTTC	XbaI
MZ110	CGAGCTCCACATAATCATTTCTATTTCGGG	SacI
MZ38	CGGGATCCATGTGTACATCTCGAAAGGCGCGT	BamHI
MZ169	CGCCCTTGCTCACCATAAGAATAGGACTCCATCTTTTTGAT	N/A
MZ170	ATCAAAAAGATGGAGTCCTATTCTTATGGTGAGCAAGGGCG	N/A
MZ171	TCCCCCGGGTTACTTGTACAGCTCGTCCATG	XmaI

Supplemental References

Fujiwara, M.T., Nakamura, A., Itoh, R., Shimada, Y., Yoshida, S., and Møller, S.G. (2004). Chloroplast division site placement requires dimerization of the ARC11/AtMinD1 protein in *Arabidopsis*. J Cell Sci **117,** 2399-2410.

Schmitz, A.J., Glynn, J.M., Olson, B.J.S.C., Stokes, K.D., and Osteryoung, K.W. (2009). *Arabidopsis* FtsZ2-1 and FtsZ2-2 are functionally redundant, but FtsZ-based plastid division is not essential for chloroplast partitioning or plant growth and development. Mol Plant **2,** 1211-1222.

Srinivasan, R., Mishra, M., Murata-Hori, M., and Balasubramanian, M.K. (2007). Filament formation of the *Escherichia coli* actin-related protein, MreB, in fission yeast. Curr Biol **17,** 266-272.